High-Resolution Incoherent Imaging of Crystals

S. J. Pennycook and D. E. Jesson
Solid State Division, Oak Ridge National Laboratory, Oak Ridge, Tennessee 37831
(Received 28 September 1989)

A Bloch-wave analysis shows how a signal dependent on the electron intensity at the atom sites can be used to form an incoherent image of a crystal structure. To a good approximation the image is given by a convolution of a compositionally sensitive object function with an appropriate resolution function, and as such can be predicted and interpreted intuitively. Information on a scale below the resolution limit can be interpreted by deconvolution.

PACS numbers: 61.16.Di, 07.80.+x

The imaging of a crystal lattice by high-resolution transmission or scanning transmission electron microscopy (STEM) has, to date, been based entirely on coherent-imaging techniques, in which bright-field or dark-field lattice images are obtained through the interference of diffracted beams.[1-4] In such phase-contrast images, the resolution and contrast are intrinsically linked and contrast reversals may occur with sample thickness or objective-lens defocus. More subtle interference effects can occur at defects and interfaces making accurate image simulation essential. In the STEM case, phase-contrast images result from interference between overlapping Bragg disks reaching the detector.[4,5] At increasing scattering angles, the coherent scattering is progressively replaced by thermal diffuse scattering.[6] Both the coherent and incoherent high-angle scattering is generated kinematically, even when the low-order diffraction is strongly dynamical, so that images formed from this may show only a weak thickness dependence. It is also more chemically sensitive since the scattering factors approach those for unscreened nuclear scattering.[7] In this paper we show how it is possible to obtain a high-resolution image showing characteristics very close to those expected for an ideal incoherent image. To a good approximation, the image is given by a convolution of a resolution function with a simple object function. Such Z-contrast images are therefore unambiguous and can be predicted and interpreted intuitively, or calculated by straightforward convolution.

These characteristics are obtained using the high-angle annular detector proposed by Howie.[8] Here we consider only the thermal-diffuse component, assuming that the inner detector angle is sufficiently high that there is negligible contribution from the coherent scattering.[9] The large scattering angle (small impact parameter) ensures that coherence between atomic columns is effectively destroyed by thermal vibrations, and the wide angular range ensures that coherent contributions from atoms at different depths in the same column are washed out.[10] Therefore, the high-angle diffuse scattering is generated by each atom in proportion to the electron intensity close to its site. As it propagates to the annular detector it may be coherently scattered by the crystal giving rise to the well-known Kikuchi-like lines seen in diffuse scattering. However, the large angular range of the annular detector will also integrate over most of this redistribution of the outgoing electrons, so that the high-angle annular detector gives a signal proportional to the integrated electron intensity at all atom sites, in a manner entirely analogous to the detection of x-ray fluorescence from crystals.[11] Clearly, in the limit of a very thin crystal, where there is no dynamical diffraction of the incident probe, an incoherent image will be formed given by the convolution of the probe intensity profile with an object function sharply peaked at the projected atomic sites. The width of the object function is determined by the average thermal vibration amplitude and impact parameter and, being typically less than 0.1 Å, can be treated as a δ function at currently available resolutions. Its strength is dependent on the number of species occupying the projected atomic sites and their atomic number Z. What is remarkable is that experimentally the incoherent character is retained even in very thick crystals when strong dynamical diffraction of the incident beam occurs as it propagates through the sample.[12]

How this occurs can be appreciated clearly using a Bloch-wave description of the coherent incident probe propagating through the crystal. The intensity at the atom sites is given by an integration over all angles contained in the incident probe. We choose a coordinate system appropriate to zone-axis diffraction in which $\mathbf{R}$ is a two-dimensional (2D) real-space vector perpendicular to the zone-axis direction $\mathbf{z}$ and $\mathbf{K}$ defines the transverse component of each electron wave vector $\boldsymbol{\chi}$ within the incident-electron probe. For a crystal consisting of atomic strings at positions $\mathbf{R}_i$ in the projected unit cell, the amplitude ψ at an atom site $(\mathbf{R}_i,z)$ due to a probe located at the surface $(\mathbf{R}_0,0)$ is given by

$$\psi(\mathbf{R}_i-\mathbf{R}_0,z)=\sum_j A^{(j)}(\mathbf{R}_i-\mathbf{R}_0,z)\,, \tag{1}$$

where the $A^{(j)}$ are amplitude contributions from each Bloch state $\tau^{(j)}$ integrated over all the angles comprising the incident probe;

$$A^{(j)}(\mathbf{R}_i-\mathbf{R}_0,z)=\int_{\text{probe}}\epsilon^{(j)}(\mathbf{K})\tau^{(j)}(\mathbf{R}_i,\mathbf{K})e^{i(s^{(j)}/2\chi)z}e^{-\mu^{(j)}(\mathbf{K})z}e^{i\mathbf{K}\cdot(\mathbf{R}_i-\mathbf{R}_0)}e^{i\gamma(\mathbf{K})}d\mathbf{K}\,. \tag{2}$$

© 1990 The American Physical Society

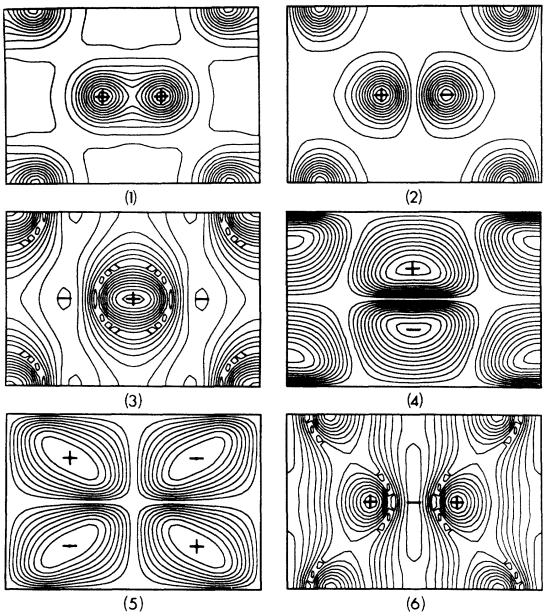

FIG. 1. The first six Bloch states for Si[110] at 100 kV (arbitrary contour intervals, phases denoted by + or − signs).

Here the $\tau^{(j)}(\mathbf{R},\mathbf{K})$ are 2D bloch states of transverse energy-band structure $s^{(j)}(\mathbf{K})$ with excitation amplitude $\epsilon^{(j)}(\mathbf{K})$ and absorption $\mu^{(j)}(\mathbf{K})$. $\gamma(\mathbf{K})$ is the usual transfer-function phase factor for spherical aberration and defocus. For high-energy electrons the more localized Bloch waves resemble 2D atomic or molecular orbital-like states for axial illumination,[13] and it is possible to assign an s- or p-type character to the states. Figure 1 shows the first six Bloch states for a 100-kV fast electron in Si[110]. Branches (1) and (2) are bonding and antibonding $1s$ states, (3), (4), and (5) are combinations of p states, and branch (6) is based on bonding $2s$ states. Since we are concerned with the intensity at the atom sites, clearly the s-type states will contribute more than the p-type states. The effect of the coherent angular integration can be predicted from the dispersion surface shown in Fig. 2. Nondispersive Bloch waves based on $1s$-type orbitals will produce a significant $A^{(j)}$, whereas the more dispersive contributions from less localized states will not add in phase. We would therefore expect the $1s$-type states to represent the dominant contribution to the amplitude at the atom sites. Treating the bonding and antibonding combinations of $1s$ states as a single effective branch (due to their small separation in transverse energy) we write the image intensity in the form

$$I(\mathbf{R}_0,t)=\sum_i\left[\int_0^t A^{(1s)^2}(\mathbf{R}_i-\mathbf{R}_0,z)\,dz + \Delta C(\mathbf{R}_i-\mathbf{R}_0,t)\right]\sigma_i\,, \quad (3)$$

where ΔC represents the dependent and independent contributions due to all other states and t is the sample thickness. In our case σ_i is a partial cross section for high-angle scattering into the annular detector which can be obtained simply from atomic cross sections.[7] With an appropriate cross section, Eq. (3) would also describe an x-ray fluorescence signal arising from a localized excitation. Figure 3 shows line traces of the image intensity in Si[110] calculated using all terms in Eq. (4), and from the first term alone. Clearly the $1s$ states are responsible for practically all of the image contrast, most of the contribution arising from the ΔC term appearing as a uni-

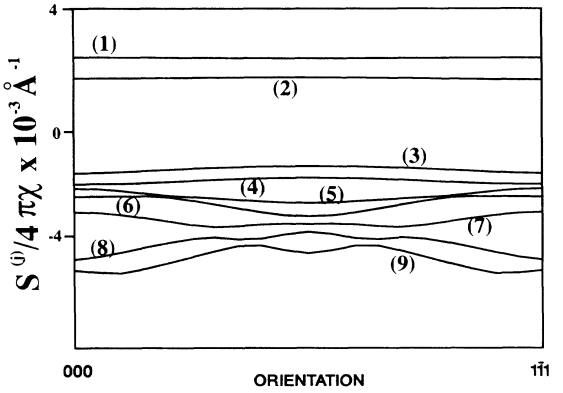

FIG. 2. Dispersion-surface section for Si[110] at 100 kV along [1$\bar{1}$1]; branches numbered in order of decreasing transverse energy.

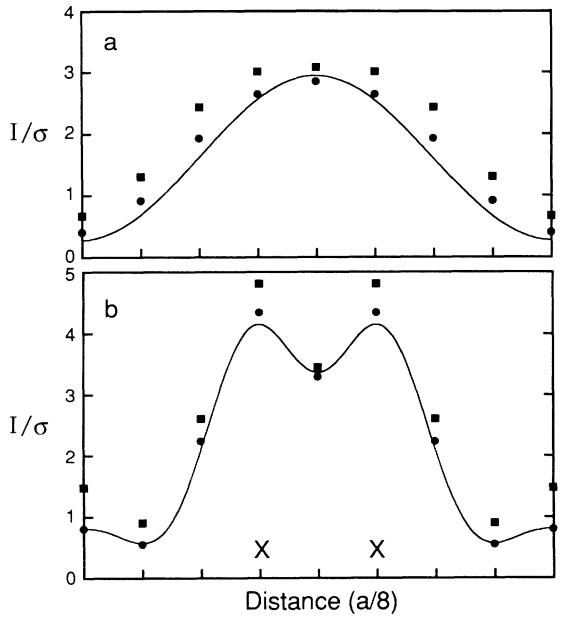

FIG. 3. Calculated line traces (normalized to cross section) from channel to channel along [001] for Si[110] using the full calculation (squares), the $1s$ states only (circles), and the effective surface-probe approximation (solid line). The crystal thickness is 20 nm, and the accelerating voltage is (a) 100 kV and (b) 300 kV. Atom sites, separated by $a/4$ (a is the lattice parameter), are represented by × on the displacement scale (Ref. 14).

form background. This first term can show no contrast reversals with defocus or sample thickness;[15] singling out such a component is the key to the realization of incoherent imaging and contrasts strongly to the situation with conventional high-resolution imaging in which all states, including those peaking between the atom sites, contribute to the image.[16] Figure 4 shows the calculated thickness dependence of the image intensity indicating good agreement with the s-state prediction at all thicknesses. Also shown are experimental measurements of the image intensity from the strings, scaled to match the calculated curve in the thickness range 20–30 nm, but agreeing well at all thicknesses.[17]

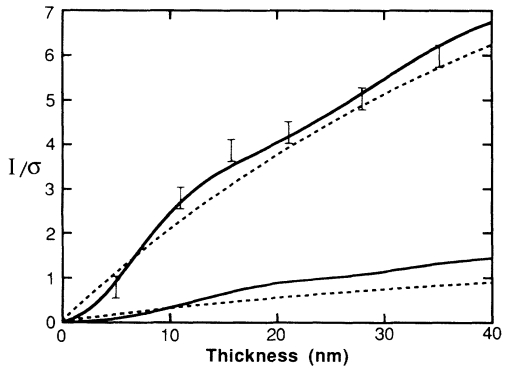

FIG. 4. Thickness dependence of the normalized image intensity calculated using the full expression (solid lines) and the 1s states only (dotted lines), for a probe located over a dumbbell (upper curves, also showing experimental points), and for a probe located over a channel (lower curves).

Since the 1s states are quite tightly bound to the atomic strings, they are relatively independent of the incident-beam direction and can be taken outside the angular integration in Eq. (2), giving in a tight-binding limit

$$I(\mathbf{R}_0,t)=\sum_i \sigma_i \left[\epsilon^{(1s)^2}(0) \left(\frac{1-e^{-2\mu^{(1s)}t}}{2\mu^{(1s)}} \right) \tau^{(1s)^2}(\mathbf{R}_i,0) P^{\text{eff}}(\mathbf{R}_i-\mathbf{R}_0)+\Delta C(\mathbf{R}_i-\mathbf{R}_0,t) \right], \tag{4}$$

where

$$P^{\text{eff}}(\mathbf{R}_i,\mathbf{R}_0)=\left| \frac{1}{\epsilon^{(1s)}(0)} \int \epsilon^{(1s)}(\mathbf{K}) e^{i\mathbf{K}\cdot(\mathbf{R}_i-\mathbf{R}_0)} e^{i\gamma(\mathbf{K})} d\mathbf{K} \right|^2 \tag{5}$$

is an effective incident-probe intensity profile taking account of the falloff in s-state excitation at high angles of incidence. The first term of Eq. (4) represents a convolution of the effective probe intensity profile with the thickness-integrated s-state intensity at the atom sites. It is shown by the solid lines in Fig. 3 and approximates very closely to the exact calculation of the first term given by Eq. (3). These results show clearly how the image contrast approximates very closely to that expected for ideal incoherent imaging. The effect of the damping envelope is primarily to reduce the peak intensity from that of the incident probe, while its width is practically unaffected. For structures consisting of identical strings, the form of the image contrast is therefore given very closely by a convolution using the incident-probe intensity profile, and as such is intuitively predictable. At 300 kV the 0.138-nm separation of the two Si columns exactly matches the Scherzer resolution limit for incoherent imaging, given by $0.43C_s^{1/4}\lambda^{3/4}$ (Ref. 1), and the predicted contrast closely matches the Rayleigh definition of the resolution limit.[18] For structures consisting of two or more strings of different strength the observed contrast is dominated by the relevant string and therefore remains intuitively predictable. These results show how Z-contrast images may be calculated accurately by simple convolution using axial Bloch states and the dispersion surface, with vast savings in computer time.

Figure 5 shows experimental images obtained with a VG Microscope's HB501 STEM operating at 100 kV using an ultrahigh-resolution pole piece of $C_s=1.3$ mm, with an incident-beam semiangle close to the optimum

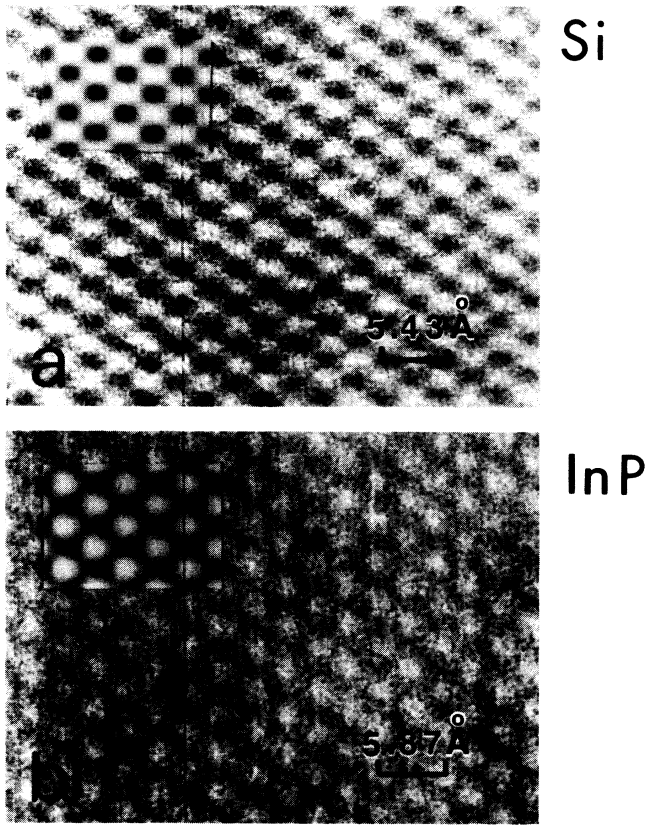

FIG. 5. Experimental Z-contrast images of (a) Si and (b) InP with images simulated using the effective surface-probe approximation shown in the inset.

10.8 mrad and detector semiangles of 75–150 mrad.[19] These agree very well with images simulated by convolution using the effective surface-probe method (shown in the inset). In Si, the two atomic columns comprising each "dumbbell," although not resolved, clearly result in an elongated image. In InP, however, where each dumbbell comprises one In column and one P column, the image is dominated by the scattering from the In column resulting in an array of almost circular bright features, better separated than in the case of Si. This is a clear indication of how information on a scale below the resolution limit is still contained in the image in a simple and predictable manner due to the incoherent nature of the image.

The independence of the s states, together with the chemical dependence arising primarily from the cross sections σ_i, gives these images compositional sensitivity on the atomic scale. In Si, the surface-probe calculations indicate that with the probe located centrally over one dumbbell 83% of the image intensity comes from that one dumbbell. The full calculation gives a value of 82%. Since the tightly bound $1s$ states are quite insensitive to states on neighboring strings, we expect that images of interfaces or superlattices could be predicted as simply as those from the perfect crystal. Compared to phase-contrast methods,[20] the strong chemical sensitivity and simple dependence on defocus and sample thickness make these images very attractive for composition mapping at atomic resolution, and indeed for all high-resolution imaging.

It is worth pointing out that the reciprocally equivalent conventional imaging mode would be high-angle hollow-cone illumination. Each atom could be considered an independent emitter and the image would again be given by the coherent angular integration over the objective aperture summed incoherently over all atoms in the sample.[21] However, this would be substantially less efficient than the STEM mode, by about 2 orders of magnitude for typical angles. Apart from possible beam-damage problems it seems unlikely that present mechanical and electronic stabilities would allow such an image to be achieved in practice.

The 300-kV STEM instruments currently under development would provide Z-contrast images with a resolution around 0.13 nm, and a simply interpretable information content to well below the 1 Å level. The strong compositional sensitivity and intuitively predictable imaging make this an attractive direction for high-resolution electron microscopy in the future.

The assistance of M. F. Chisholm is gratefully acknowledged. This research was sponsored by the Division of Materials Sciences, U.S. DOE, under Contract No. DE-AC05-84OR21400 with Martin Marietta Energy Systems, Inc., and was supported in part by the U.S. DOE Postgraduate Research Program administered by the Oak Ridge Associated Universities, Inc.

[1]O. Scherzer, J. Appl. Phys. **20**, 20 (1949).

[2]E. Zeitler and M. G. R. Thomson, Optik **31**, 258 (1970).

[3]J. M. Cowley, Ultramicroscopy **2**, 3 (1976).

[4]J. C. H. Spence and J. M. Cowley, Optik **50**, 129 (1978).

[5]E. J. Kirkland, R. F. Loane, and J. Silcox, Ultramicroscopy **23**, 77 (1987); R. F. Loane, E. J. Kirkland, and J. Silcox, Acta Cryst. A **4**, 912 (1988).

[6]C. R. Hall and P. B. Hirsch, Proc. Roy. Soc. (London) A **286**, 158 (1965).

[7]S. J. Pennycook, S. D. Berger, and R. J. Culbertson, J. Microsc. **144**, 229 (1986).

[8]A. Howie, J. Microsc. **117**, 11 (1979). For a review of previous applications, see M. M. J. Treacy and S. B. Rice, J. Microsc. (to be published); Pennycock, Berger, and Culbertson, Ref. 7.

[9]This is an overstringent requirement since the coherent component at high scattering angles also results in similar image characteristics, D. E. Jesson and S. J. Pennycook (to be published).

[10]J. M. Gibson and A. Howie, Chem. Scr. **14**, 109 (1978).

[11]D. Cherns, A. Howie, and M. H. Jacobs, Z. Naturforsch **28a**, 565 (1973).

[12]S. J. Pennycook and L. A. Boatner, Nature (London) **336**, 565 (1988); S. J. Pennycook, Ultramicroscopy **30**, 58 (1989).

[13]K. Kambe, G. Lehmpfuhl, and F. Fujimoto, Z. Naturforsch **29a**, 1034 (1974).

[14]Images are calculated for an objective-lens spherical-aberration coefficient $C_s = 1.3$ mm with optimum illumination angle, $(4\lambda/C_s)^{1/4}$, and defocus, $-(C_s\lambda)^{1/2}$ ($\lambda = 2\pi/\chi$), using 1315 incident orientations. 63 and 91 beams were used at 100- and 300-kV accelerating voltage, respectively.

[15]At high defocus values the probe shows strong subsidiary maxima which can result in reversed images, although showing much weaker contrast.

[16]K. Kambe, Ultramicroscopy **10**, 223 (1982).

[17]The contrast was difficult to measure due to noise limitations, but appeared weaker than expected. This could be due to a number of effects including the neglect of the high-angle scattering from absorbed electrons, probe instabilities, or probe broadening in an amorphous surface layer.

[18]M. Born and E. Wolf, *Principles of Optics* (Pergamon, Oxford, 1986), 6th ed., p. 415.

[19]The total coherently scattered intensity in the high-order Laue-zone reflections is less than 1% of the total intensity reaching the annular detector.

[20]A. Ourmazd, D. W. Taylor, J. Cunningham, and C. W. Tu, Phys. Rev. Lett. **62**, 933 (1989).

[21]In principle, this would also allow the possibility of energy-filtered incoherent images.

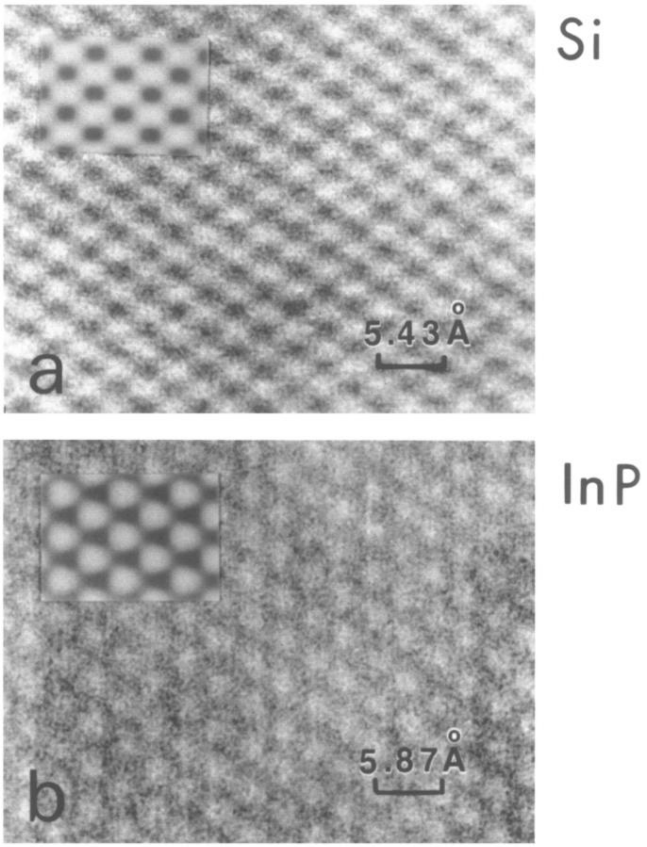

FIG. 5. Experimental Z-contrast images of (a) Si and (b) InP with images simulated using the effective surface-probe approximation shown in the inset.